Available online at www.sciencedirect.com
ScienceDirect
Journal of Physics and Chemistry of Solids 67 (2006) 2192–2196
JOURNAL OF PHYSICS AND CHEMISTRY OF SOLIDS
www.elsevier.com/locate/jpcs

Nonhydrostatic compression of bismuth to 222 GPa: Some constraints on elasticity of the bcc-phase

A.K. Singh[a,*], E. Menéndez-Proupin[b], G. Gutiérrez[b], Y. Akahama[c], H. Kawamura[c]

[a]*Materials Science Division, National Aerospace Laboratories, Bangalore 560 017, India*
[b]*Department of Physics, Faculty of Science, Universidad de Chile, Casilla 653, Santiago, Chile*
[c]*Faculty of Science, Himeji Institute of Technology, Hyogo 678-1297, Japan*

Abstract

Polycrystalline bismuth sample was compressed in a diamond anvil cell and X-ray diffraction patterns from the body centered cubic phase of bismuth (bcc-Bi) recorded in the pressure range 12–222 GPa. The analysis of diffraction data indicates that the factor $S = (S_{11}-S_{12}-S_{44}/2)$ is positive, where S_{ij} are the single-crystal elastic compliances. The data suggest $S/S_{11} \cong 0.5$ in the entire pressure range if stress continuity across the grain boundaries is assumed, and $S/S_{11} \cong 0.9$ if a condition halfway between the stress and strain continuities is assumed. These results are compared with the first principle calculations of the elastic moduli carried out recently. The upper bound of the uniaxial stress component (the difference between the axial and radial stress components) increases linearly from very low value at 12 to ≈ 3 GPa at 222 GPa.

Keywords: A. Metals; C. High pressure; C. X-ray diffraction; D. Phase transition; D. Elastic properties

1. Introduction

Bismuth is rhombohedral (A7) at ambient pressure and undergoes a number of structural phase transitions as the pressure is increased and acquires a body centered cubic phase at 7.7 GPa [1, and references therein]. The calculation of structure dependent part of cohesive energy using pseudopotential method [2] showed that the bcc-Bi is more stable than other commonly encountered structures such as hexagonal close packed, face centered cubic, and simple cubic down to compression of $V/V_0 = 0.5$. The volume compression measurement by high-pressure X-ray diffraction [3] showed that the bcc-Bi was indeed stable up to 222 GPa that corresponded to a measured compression of $V/V_0 = 0.4735 \pm 0.001$. Because of the high compressibility of bcc-Bi, its use as a pressure marker in high-pressure X-ray experiments was suggested. The single-crystal elastic moduli of the high-pressure phases are obtained through the first-principle calculations and measurement thereof has remained a challenge. Analysis of the powder diffraction data under nonhydrostatic compression offers the only way of measuring single-crystal elastic moduli of the high-pressure phases [4–6]. However, this method requires diffraction data taken with the radial [7] or perpendicular [8] geometry. Several examples [8–10] of such studies can be found in literature. In particular, studies on the elasticity of hcp-Fe [11] and of $CaCl_2$-phase of silica [12] are examples of measurements on the phases that are stable only under pressure. The diffraction experiments on bcc-Bi conducted earlier [3] used the conventional geometry that does not give the range of data required for the estimation of elastic moduli. In this paper, we analyze the line-shift and line-width data obtained earlier [3] to constrain $(S_{11}-S_{12}-S_{44}/2)$ of bcc-Bi up to 222 GPa. This is an example of the information on single-crystal elasticity that can be obtained from the data obtained using conventional geometry. The results of this study have been compared with those obtained from the first-principle calculation (FPC) of elastic moduli

*Corresponding author.
E-mail address: aksingh@css.nal.res.in (A.K. Singh).

0022-3697/$ - see front matter © 2006 Elsevier Ltd. All rights reserved.
doi:10.1016/j.jpcs.2006.06.002

in the framework of DFT with GGA and pseudopotentials [13].

2. Experimental details

X-ray diffraction experiments were performed using diamond anvil cell (DAC) with anvil face of 50 μm. The polycrystalline Bi and Pt samples, both in foil form, were stacked and loaded in Re gasket. The thickness of the indented region and diameter of the central hole were 18 and 35 μm, respectively. The incident beam (wavelength $\lambda = 0.03292$ nm) from beam line BL04B2 at SPring-8 was collimated to 25 μm. Typical exposure times were 900 s. Diffraction patterns were recorded on an image plate and the images analyzed using the integration software PIP [14]. The pressures were estimated using the equation of state of Pt [15].

3. Method of data analysis

The solid sample compressed in a DAC undergoes considerable plastic deformation and develops a highly complex stress state. The strains produce by such stresses can be conveniently computed by considering the stress state as a superposition of two types of stresses—macro- and micro-stresses. Macro-stresses produce strains that cause the diffraction lines to shift whereas the strains produced by micro-stresses result in diffraction-line broadening. The macro-stresses at the center of the sample possess axial symmetry about the load axis of the DAC. The lattice strains produced by such a stress state have been examined in detail in earlier studies [4–6]. For the cubic system, the lattice parameter obtained from different reflections recorded with the conventional diffraction geometry satisfies the following relation [16]:

$$a_m(hkl) = M_0 + M_1[3\Gamma(hkl)(1 - 3\sin^2\theta)], \quad (1)$$

where

$$M_0 = a_P\{1 + (\alpha t/3)(1 - 3\sin^2\theta) [(S_{11} - S_{12}) - (1 - \alpha^{-1})(2G_V)^{-1}]\},$$
$$M_1 = -a_P(\alpha St/3),$$
$$\Gamma(hkl) = (h^2k^2 + k^2l^2 + l^2h^2)/(h^2 + k^2 + l^2)^2,$$
$$S = (S_{11} - S_{12} - S_{44}/2).$$

S_{ij} are the elastic compliances and θ is the diffraction angle. The difference between the axial and radial stress components, termed uniaxial stress component, is denoted by t. G_V is the shear modulus of the randomly oriented polycrystalline aggregate under iso-strain (Voigt) condition. It may be noted that the angle ψ between the diffraction vector and load axis of the DAC equals $(\pi/2-\theta)$ for the conventional diffraction geometry. To a good approximation, $M_0 \cong a_p$, and the $a_m(hkl)$ versus $3(1 - 3\sin^2\theta)\Gamma(hkl)$ plot, termed gamma plot, is a straight line. The following relation can be used to determine αSt from the gamma plots,

$$\alpha St = -3M_1/M_0. \quad (2)$$

The term α decides the weights of shear moduli under the conditions of stress continuity (Reuss) and strain continuity (Voigt) across the grain boundaries in the polycrystalline aggregate. $\alpha = 1$ corresponds to the condition of stress continuity while $\alpha = 0.5$ corresponds to a condition halfway between the conditions of stress and strain continuities. The possible values that α can assume under high-pressure condition were discussed in earlier publications [5–7]. However, we retain α in Eq. (2) and discuss its effect on the results later in this paper.

The theory proposed earlier [17,18] for diffraction-line broadening from deformed metals was modified [19,20] to yield the following relation:

$$(2w_{hkl}\cos\theta)^2 = (\lambda/d)^2 + \eta^2_{hkl}\sin^2\theta_{hkl}, \quad (3)$$

where $2w_{hkl}$ is the full width at half maximum (FWHM) of the diffraction profile on 2θ-scale and corrected for the instrumental broadening. The symbols d, λ, and η_{hkl} denote grain size, X-ray wavelength, and the micro-strain, respectively. Grain size is considered independent of (hkl) and is determined from the intercept of the plot. Micro-strain can be then determined for each reflection from the following relation:

$$\eta^2_{hkl} = [(2w_{hkl}\cos\theta)^2 - (\lambda/d)^2]/\sin^2\theta. \quad (4)$$

The (hkl)-dependence of η_{hkl} is given by [17]

$$\eta_{hkl} = 4p_{max}[S_{11} - 2S\Gamma(hkl)]. \quad (5)$$

The results on MgO [20] and many other materials suggest that $2p_{max} = t$. Eq. (5) reduces to

$$\eta_{hkl} = 2t[S_{11} - 2S\Gamma(hkl)]. \quad (6)$$

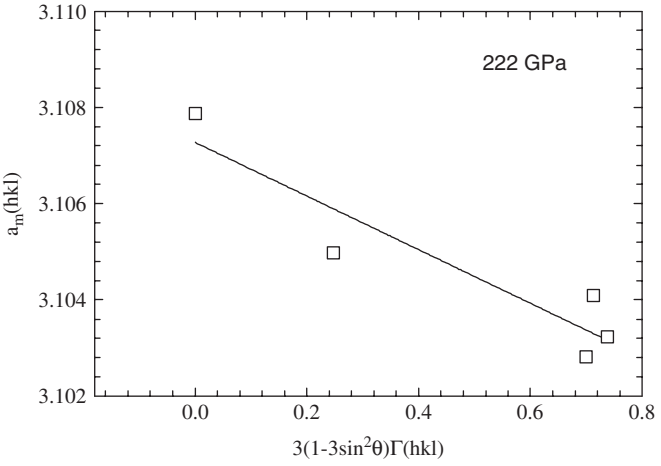

Fig. 1. An example of gamma plot.

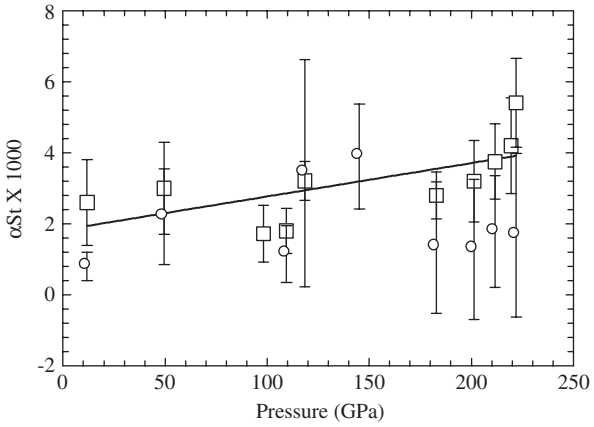

Fig. 2. αSt derived from the gamma plots are shown by unfilled squares. St derived from the line width analysis [Eq. (6)] are shown by unfilled circles. The line shows least-squares fit through unfilled squares.

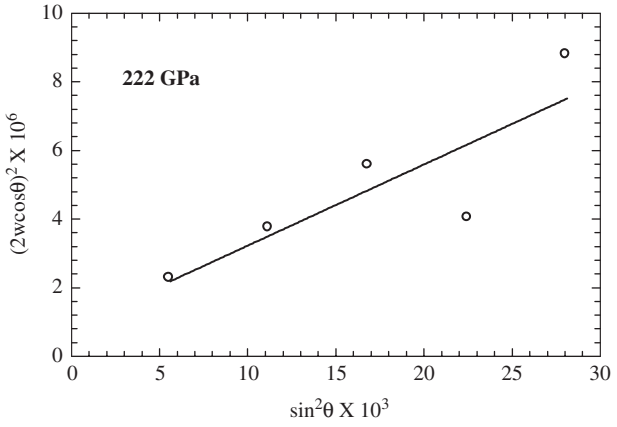

Fig. 3. The typical $(2w\cos\theta)^2$ versus $\sin^2\theta$ plot.

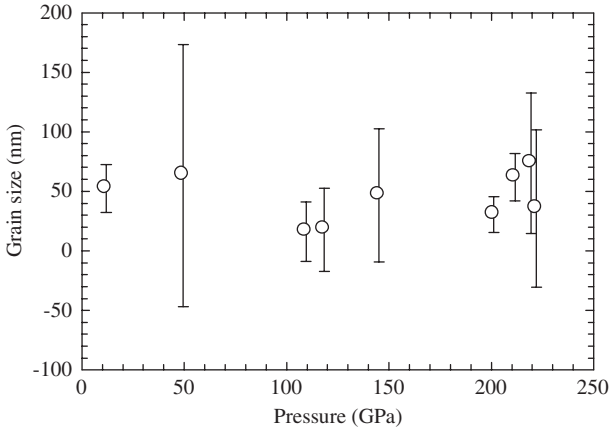

Fig. 4. The grain sizes at different pressures.

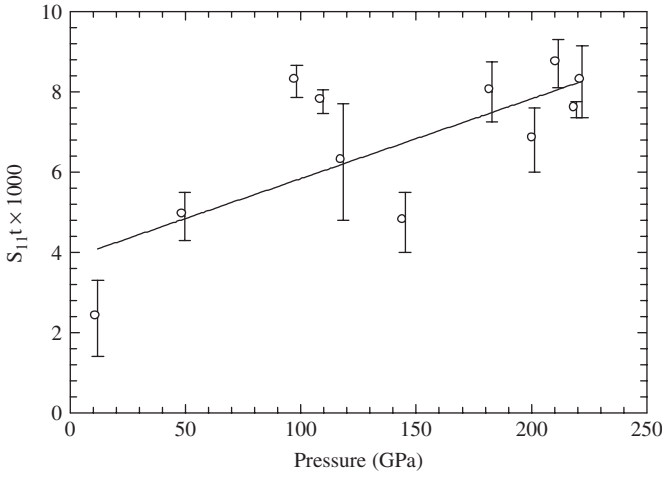

Fig. 5. $S_{11}t$, derived from the line width analysis at different pressures.

4. Results

A total of 11 runs in the pressure range 12–222 GPa were selected for the present analysis. In each run the first five reflections from the bcc-Bi were observed. The gamma plots were constructed for each run. A typical plot is shown in Fig. 1. The gamma plot in one run showed no systematic trend and was ignored. The αSt-values computed using Eq. (2) for the remaining 10 runs are shown in Fig. 2. The measured FWHM were used to construct the $(2w\cos\theta)^2$ versus $\sin^2\theta$ plots. Typical plot is shown in Fig. 3. The data in two runs showed no trend in such plots. For the remaining nine runs the grain sizes were computed from the intercepts of such plots and are shown in Fig. 4. The strains were computed from Eq. (4). The St and $S_{11}t$ computed using Eq. (6) are shown in Figs. 2 and 5, respectively.

5. Discussion

In the present experiments, significant proportion of the diffracted intensity arose from the region of pressure gradient as the incident X-ray beam illuminated large area of the sample. Eqs. (1) through (6) do not take into account the effect of large pressure gradients. We proceed with the discussion of the results keeping in mind this limitation.

The average grain size is found to be 50 nm and is nearly pressure independent. Since the line widths were not corrected for the instrumental broadening, the grain sizes are systematically underestimated. Further, the errors in the estimation of grain sizes are large, the standard error being comparable to the magnitude of the grain size itself. This is the direct outcome of the use of short wavelength in the diffraction experiments with a DAC. A short wavelength radiation as the primary beam is essential to overcome the absorption in the diamond anvils and to allow sufficient number of reflections through the narrow window available for emergence of the diffracted beam from the DAC. The large errors in the estimates of grain sizes are therefore inherent in such experiments.

In the high-pressure region, the values of St derived from the line-width analysis are consistently much lower than αSt values obtained from the line-shift analysis (Fig. 2). However, all values St or αSt are positive. Noting that t is

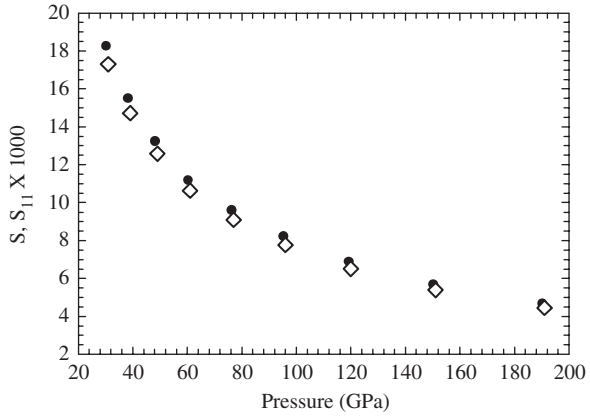

Fig. 6. Filled circles and unfilled diamonds show S and S_{11} derived from the elastic moduli obtained from the first-principle calculations.

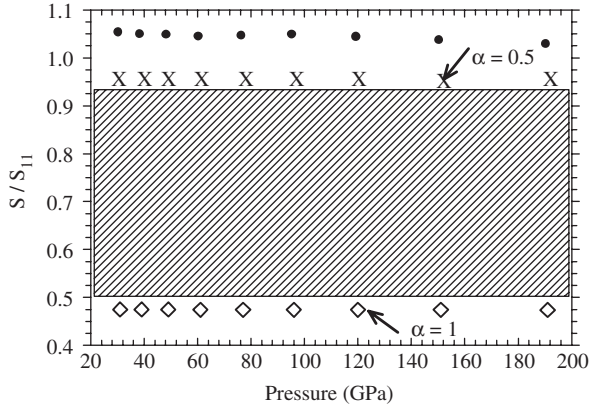

Fig. 7. A comparison of S/S_{11} obtained from the present analysis with that obtained from the first-principle calculations (filled circles). Diamonds indicate the values derived from experimental data with $\alpha = 1$. As α is reduced, the values shift through the shaded region to the values marked by crosses at $\alpha = 0.5$.

taken positive by convention, the results suggest that S for bcc-Bi is positive in the pressure range of 12–222 GPa. It is seen from Fig. 5 that the values of $S_{11}t$ are positive, as expected.

Fig. 6 shows the values S and S_{11} derived from the elastic moduli obtained from the FPC [13]. It is seen that the S is large positive at 31 GPa, the first pressure point of calculation, and decreases with increasing pressure but remains positive up to $\approx$200 GPa. The sign of S deduced from the X-ray diffraction data are in agreement with the results of FPC. Further, it is seen from Fig. 6 that the computed S_{11} is close to S in the entire pressure range suggesting that $S/S_{11} \cong 1$. Though the errors in the estimations of αSt and $S_{11}t$ are large, it is tempting to derive the ratio $\alpha S/S_{11}$ from the data in Figs. 2 and 5. Fig. 7 shows the S/S_{11}-values from FPC and those calculated from the straight-line fits to the data in Figs. 2 and 5. It is seen that the values derived from experimental data with $\alpha = 1$ are significantly lower than the results of FPC while

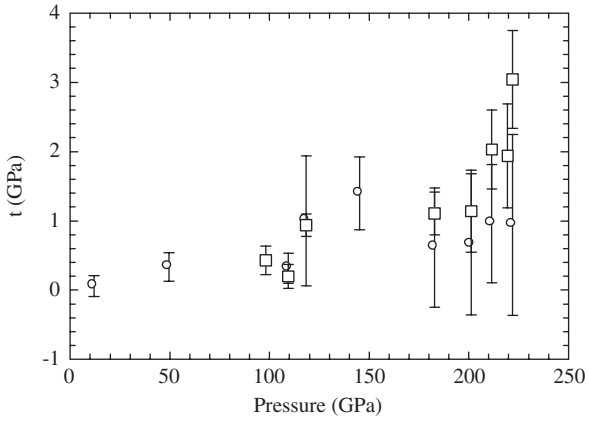

Fig. 8. The pressure dependence of t obtained using line-shift data (unfilled squares) and line-width data (unfilled circles).

the values with $\alpha = 0.5$ show much better agreement with the results of FPC. This may be taken as an indication of the fact that $\alpha = 0.5$ provides a better description of the nonhydrostatic part of the stress state. It is to be noted that S for bcc-Bi is large, being 0.028 GPa^{-1} at 12 GPa. In an earlier study on Au, which also has large S, the choice of $\alpha = 0.5$ resulted in a better agreement between the results obtained from X-ray diffraction technique and those extrapolated of the ultrasonic data [7]. The uniaxial stress component t can estimated from the measured αSt using $\alpha = 0.5$ and $S_{11}t$ as the S and S_{11} values are obtained from the FPC. The $t-P$ data are shown in Fig. 8. It is seen that t is small at 12 GPa and reaches 3 GPa at 222 GPa.

6. Conclusions

This paper provides an example of study that can be carried out with X-ray diffraction data limited over small range of ψ. The sign of S and magnitude of S/S_{11} derived from the diffraction data are in agreement with the results of the first-principle calculation of elastic moduli. The upper bound of the uniaxial stress component is $\approx$3 GPa at 222 GPa. This indicates that the stress state in bcc-Bi does not deviate appreciably from hydrostatic even at such high pressures.

Acknowledgements

AKS acknowledges the support he received from the Director, NAL. E. M-P. and G. G. received support from FONDECYT (Chile) Grant nos. 1050293 and 1030063, respectively.

References

[1] M.I. McMahon, O. Degtyareva, R.J. Nelmes, Phys. Rev. Lett. 85 (2000) 4896.
[2] K. Aoki, S. Fujiwara, Kusakabe, J. Phys. Soc. Japan 51 (1982) 3826.
[3] Y. Akahama, H. Kawamura, A.K. Singh, J. Appl. Phys. 92 (2002) 5892.

[4] A.K. Singh, J. Appl. Phys. 73 (1993) 4278.
[5] A.K. Singh, H.K. Mao, J. Shu, R.J. Hemley, Phys. Rev. Lett. 80 (1998) 2157.
[6] A.K. Singh, C. Balasingh, H.-K. Mao, R.J. Hemley, J. Shu, J. Appl. Phys. 83 (1998) 7567.
[7] T.S. Duffy, G. Shen, D.L. Heinz, J. Shu, Y. Ma, H.K. Mao, R.J. Hemley, A.K. Singh, Phys. Rev. B 60 (1998) 15063.
[8] H.K. Mao, R.J. Hemley, High Pressure Res. 14 (1996) 257.
[9] S. Merkel, H.R. Wenk, J. Badro, G. Montagnac, P. Gillet, H.K. Mao, R.J. Hemley, J. Geophys. Res. 107 (2002) 2271 (No B11).
[10] T.S. Duffy, G. Shen, J. Shu, H.K. Mao, R.J. Hemley, A.K. Singh, J. Appl. Phys. 86 (1998) 6729.
[11] H.K. Mao, J. Shu, G. Shen, R.J. Hemley, B. Li, A.K. Singh, Nature (London) 396 (1998) 741.
[12] S.R. Shieh, T.S. Duffy, Phys. Rev. Lett. 89 (2002) 25507.
[13] G. Gutiérrez, E. Menéndez-Proupin, A.K. Singh, J. Appl. Phys. 99 (2006) 103504.
[14] O. Shimomura, K. Takemura, H. Fujihisha, Y. Fujii, Y. Ohishi, T. Kikegawa, Y. Amemiya, T. Matsushita, Re. Sci. Instrum. 63 (1992) 967.
[15] N.C. Holmes, J.A. Moriarty, G.R. Gathers, W.J. Nellis, J. Appl. Phys. 66 (1989) 2962.
[16] A.K. Singh, K. Takemura, J. Appl. Phys. 90 (2001) 3269.
[17] A.R. Stokes, A.J.C. Wilson, Proc. Phys. Soc. (London) 56 (1944) 174.
[18] J.I. Langford, J. Appl. Cryst. 4 (1971) 164.
[19] A.K. Singh, J. Phys. Chem. Solids 65 (2004) 1589.
[20] A.K. Singh, H.P. Liermann, S.K. Saxena, Solid. State. Commun. 132 (2004) 795.